"This document is the Accepted Manuscript version of a Published Work that appeared in final form in ACS Applied Nano Materials, copyright © American Chemical Society after peer review and technical editing by the publisher. To access the final edited and published work see https://pubs.acs.org/doi/abs/10.1021/acsanm.9b02596."

Supported AuCu Alloy Nanoparticles for the

Preferential Oxidation of CO (CO-PROX)

Tanna Elyn Rodrigues Fiuza, Daniela Zanchet*

Institute of Chemistry, University of Campinas (UNICAMP), P.O. Box 6154, 13083-970

Campinas, São Paulo, Brazil

KEYWORDS: AuCu, CO-PROX, alloy nanoparticles, bimetallic nanoparticles, nanocatalysis,

CO oxidation, hydrogen production

ABSTRACT: The insertion of copper into the gold lattice forming gold-copper (AuCu)

nanoalloys enhances the gold catalytic performance in reactions such as CO oxidation. Here, we

compared the catalytic performance of 6 nm AuCu nanoparticles (NPs) supported on SiO₂

(AuCu SiO₂), a non-reducible oxide, and CeO₂ (AuCu CeO₂), a reducible one, under

preferential oxidation of CO (CO-PROX). Under reaction conditions, the support nature

impacted in the stabilization of different species on the catalyst surface. The AuCu CeO2 was

both more active and more stable, which was associated with the ability of CeO2 to stabilize the

AuCu alloy phase under reaction conditions.

1

1. Introduction

The control of the size and shape of the noble metal nanoparticles (NPs) dispersed on high surface area supports has a clear impact on the catalytic performance of the system since it determines the facets and the low-coordinated sites that are exposed and can lead to the formation of unique interfacial sites, tuning the reactivity of the catalyst.¹⁻⁷ In addition, its combination with a second non-noble metal forming bimetallic NPs has attracted much attention and examples of superior performance have been found in several reactions. Bimetallic NPs can be synthesized with tunable chemical ordering, such as alloy (random or chemically ordered), core-shell and Janus^{8,9} NPs. The final chemical ordering depends on the thermodynamics¹⁰ as well as on the synthetic parameters.¹¹ In bimetallic catalysts, it is important to consider ensemble (geometric) and ligand effects.¹²⁻¹⁵ The first effect is related to the particular arrangement/composition of an ensemble of metal atoms on the surface, in which the reactants will be adsorbed.^{13,14} The second effect is related to the changes in the chemical properties due to the electronic perturbations caused by strain and/or a direct charge transfer between the metals.^{13,14,17} These variations lead to changes in the adsorption energies, and consequently in the reaction rate.¹⁶⁻¹⁸

The Au-based nanoalloys have presented promising results in several catalytic reactions.¹⁹ In the case of CO oxidation (OX-CO), for example, density functional theory (DFT) calculations showed that in AuCu alloys, CO activation takes place on Au atoms while the O₂ species are activated on Cu-rich sites.¹⁹ This bifunctional mechanism enhances the catalytic activity of the alloy in comparison with monometallic Au.¹⁹ The increase of Cu content in AuCu alloys lead to an upper shift of the *d-band* center compared to monometallic Au, increasing the binding strength of intermediates, such as COOH and CO on CO₂ reduction, for example.²⁰ These

changes in the electronic structure, combined with the geometric effects, in which Au-Cu neighbor atoms can better stabilize the intermediates, determines the optimum Au:Cu ratio for a given reaction. In other words, the presence of an M metal in the host N lattice forming M-N nanoalloys changes the chemisorption properties, impacting on the surface properties by affecting the adsorption sites that may improve the catalytic performance.²¹

In nanoalloys, it is also important to consider that unique structures can be energetically favored. Guisbiers et al.22 reported their theoretical and experimental results of various AuCu polyhedra in the range of 4 and 10 nm size indicating that enrichment of Au at the surface is energetically favored. However, it is important to note that the presence of ligands in the NPs surface and the interaction with supports impact the surface energy balance, and can modify the trend of metal segregation in nanoalloys. 22,23 In addition, the reaction conditions can provide a strong driving force for metal segregation. In the case of Au-Me alloys in which "Me" is a transition metal such as Ni and Cu, an oxidative treatment leads to the enrichment of these metals on the catalysts surface forming MeO_x species.^{23,24} The segregation of the AuCu alloy forming Au-rich NPs and CuO_x species under oxidative conditions was previously reported in the literature. ^{25–32} Liu et al. ²⁷ showed that the formation of an Au-CuO_x-SiO₂ interface improved the sintering resistance of the Au NPs on SiO₂ and enhanced the catalyst performance in OX-CO through a bifunctional mechanism. Zhan et al.³¹ showed that chemical ordering (random alloy vs. chemically ordered alloy) also affected the dealloy process, in which the chemically ordered alloy was more stable under similar conditions. Najafishirtari et al.^{25,29} evaluated the impact of redox pretreatments on AuCu NPs supported on Al₂O₃ and AuCu@Fe₂O₃ dumbbells and showed that a reducing pretreatment reduced the CuO_x species and favored the partial AuCu re-alloying, in agreement with other reports in literature. 27,28,31-34 Destro et al. 30 compared in detail AuCu/SiO₂ and AuCu/Al₂O₃ catalysts, showing that the support nature played a crucial role in the Cu alloy/de-alloy process and in stabilizing different species under reactional atmosphere.³⁰ While the CuO_x species formed under the oxidative atmosphere remained mostly in the vicinity of the Au NPs when supported on SiO₂, in Al₂O₃ they spread all over the support surface. This impacts the final Cu distribution in the alloy NPs after the reducing pretreatment.³⁰

In the case of reducible oxides, such as CeO₂, the scenario is more complex: besides the indirect role in the stabilization of different catalytic species on the surface, these oxides may also participate in the reaction through a bifunctional mechanism, according to the reaction. 35-40 CeO₂ is widely used as support in catalysis due to its well-known oxygen storage capacity. Depending on the reaction conditions, the lattice oxygen of CeO₂ can be released and oxidize species, forming oxygen vacancies that can also act as adsorption sites, leading to the dissociation of adsorbed species. 41-44 The surface vacancies can also help to stabilize the metallic phase against sintering. 45 CeO₂ is common to support in Au-based catalysts since the CeO₂ vacancies allow the activation of O₂ species which are not easily activated on the metallic surface. Regarding the CO oxidation (especially under H2-rich atmosphere - CO-PROX), CuO_x/CeO₂ system has been also widely studied due to its high activity and selectivity toward CO₂ in comparison with non-reducible supports (i.e. CuO_x/SiO₂).⁴⁰ It has been proposed that Cu- CeO_2 interaction in CuO_x/CeO_2 system leads to the formation of the $Cu^{2+} \leftrightarrow Cu^+$ and $Ce^{3+} \leftrightarrow Cu^+$ Ce4+ redox pairs, associating the Cu+ as the active site to CO adsorption.46,47 Nevertheless, Caputo et al. 48 demonstrated via temperature-programmed experiments that the presence of small amounts of Cu shifted the reduction events of CeO₂ to lower temperatures compared to the bare support, promoting the oxidation of CO by the oxygen from the support at a lower temperature. By increasing the temperature, Cu⁰ was formed decreasing the catalytic performance of CuO_x/CeO₂ catalysts in CO-PROX reaction, since the reduced Cu favors the undesired and parallel H₂ oxidation. These results agree with other reports in literature.^{49–51}

Although the effect of the reducible oxides in the catalytic performance and stabilization of different species under reaction conditions have been extensively studied, there is limited and apparently conflicting information about their impact in the stabilization of AuCu NPs and in the catalytic performance of this system in CO-PROX reaction. For example, Barroso-Martín et al. 52 studied the role of light irradiation in enhancing the CO-PROX reaction; the best results were obtained with AuCu alloy supported on Ti-SBA under irradiation but the formation of AuCu alloy increased the catalytic performance in comparison with the non-reduced catalysts, even in dark or in the absence of Ti. Li et al. 26 on the other hand, studied an Au/CuO/SBA-15 catalyst and proposed that the formation of the AuCu alloy under reaction conditions led to catalyst deactivation; however, they mentioned that the Au/CuO/SBA-15 system was complicated and further studies would be required. Kandoi et al.⁵³ presented an interesting theoretical study by periodic density functional theory (DFT) calculations and micro-kinetic modeling of CO-PROX reaction, comparing the selectivity towards CO₂ on Au(111), Cu(111) and Pt(111). The selectivity towards CO₂ was dependent on the CO and H₂ oxidation reaction rates and the surface coverage. In the case of Au and Cu, the authors found similar selectivity (100 %) for both metals at 423 K, despite the differences in the ratio of the coverage of adsorbed CO and H and the constant rates of the forward reactions for CO and H2 oxidation. At 823 K, the surface CO/H coverage ratio on both metals decreased, but it was more significant on Au(111) leading to a lower selectivity towards CO₂ in comparison with Cu(111). This compensating effect, between surface coverage and reaction rates, will probably take place on the AuCu alloy, although this was not addressed in their work. Fiorenza et al.⁵⁴ prepared an Au-Cu/CeO₂ catalyst and the

monometallic counterparts by deposition-precipitation and applied to CO-PROX reaction: the Au-Cu/CeO₂ catalyst presented a slightly better performance than Au/CeO₂, while the Cu/CeO₂ catalyst presented lower activity at lower temperature but higher CO conversion and selectivity at higher temperature than Au-Cu/CeO₂. The authors were not able to associate the catalytic performance with the formation of the AuCu alloy; the lack of XRD peaks corresponding to the metallic phase indicated the occurrence of highly dispersed species. Jing et al.55 prepared Au_x/CeO₂-CuO catalysts with different Au/Cu atomic ratio by coprecipitation method and showed that the Au promoted the CO adsorption and enhanced the activity and stability of the CeO₂-CuO catalyst. Different results were shown by Laguna et al.⁵⁶; the presence of Au did not impact significantly the activity in CO-PROX reaction and, in fact, slightly decreased the CO conversion at higher temperatures. Liao et al.⁵⁷ evaluated the impact of the Cu/Au ratio (1:3, 1:1 and 3:1) and pretreatment in AuCu/CeO₂ catalysts prepared by Cu impregnation on Au-CeO₂; the reduced catalysts presented better catalytic activity than the calcined catalysts and were stable on stream. Liu et al.⁵⁸ reported that the catalytic performance of AuCu supported on silica gel was dependent on the Au:Cu ratio and these catalysts were more active than the monometallic counterparts. Potemkin et al.⁵⁹ found that, at low temperatures, the CO conversion of AuCu/CeO2 was similar to the physical mixture of Au/CeO2 and Cu/CeO2 and slightly lower than Au/CeO₂; above 150 °C, the AuCu/CeO₂ performed better with increased selectivity toward CO₂ compared to Au. Fonseca et al. 60, on the other hand, proposed that the Au-CuO_x/CeO₂ was the stable phase in their system under CO-PROX and presented good activity (comparable to Au/CeO₂) and good selectivity (comparable to Cu/CeO₂). Other works showed that CuO_x/CeO₂ was active in CO-PROX, but is deactivated by the formation of metallic Cu that favored the H₂ oxidation. ^{49–51,61} Scirè et al. ⁶² highlighted the impact of the preparation method and pretreatments

in the performance of Au/CeO₂ and Cu/CeO₂ in CO-PROX. It is very likely that the complexity of the AuCu system is related to the synthesis method and the difficulties to characterize the catalysts, in particular, the presence of atomically dispersed species on the supports and the coexistence of monometallic nanoparticles.

In this work, the main goal was to shed light on the impact of the support nature (reducible vs. non-reducible) and the conditions (reducing and oxidizing) in the stability of the AuCu alloy and how these parameters were related to the catalytic performance in CO-PROX. This reaction takes place under reducing conditions and favors the stabilization of the alloy phase. To achieve this goal, we used colloidal AuCu NPs with well-defined size and shape as a strategy to produce comparable CeO₂ and SiO₂ supported catalysts by eliminating the role of the support on the initial nucleation and growth of the metallic phase that could lead to the formation of different populations of atomically-disperse species and co-existence of monometallic NPs. Structural changes under oxidative and reductive pretreatments were followed by in situ X-ray diffraction (XRD) and XAFS (X-ray absorption fine structure spectroscopy). The catalysts were evaluated for CO-PROX reaction after being submitted to different pretreatments, aiming to understand in detail the role of the supports in the stabilization of the active species under reaction conditions.

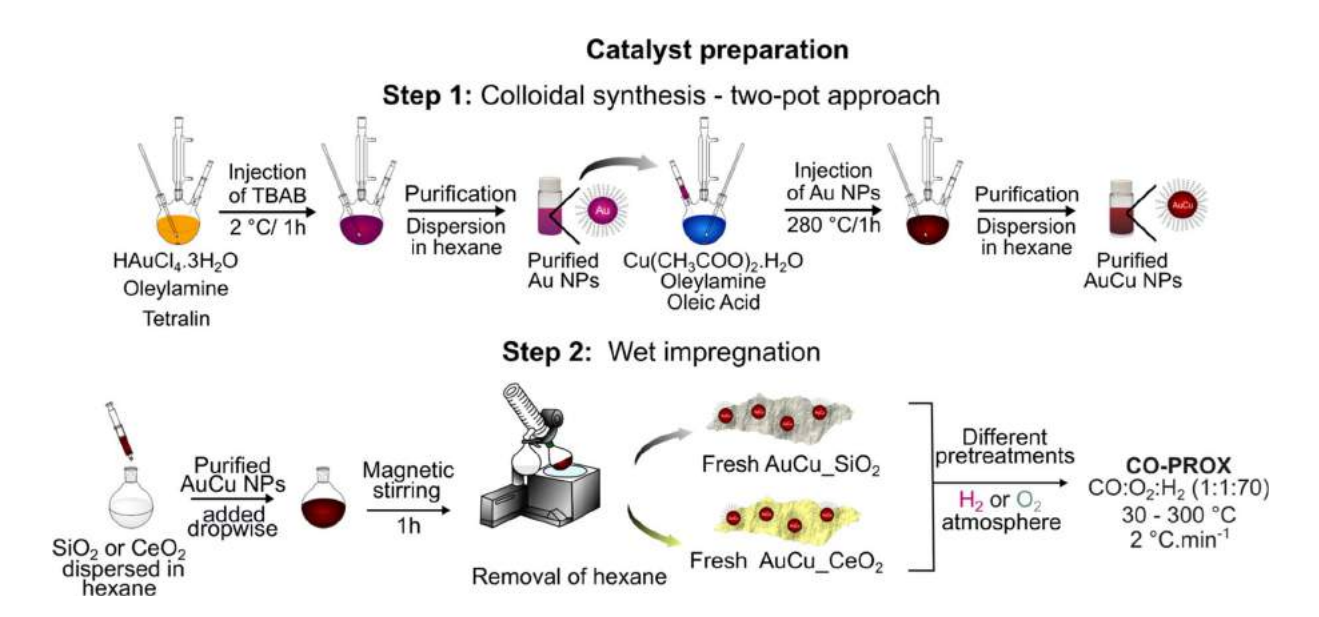
2. Experimental Section

Schema 1 summarizes the catalyst preparation, from the colloidal synthesis of the AuCu NPs (Step 1) to the catalyst preparation, which includes the impregnation of the AuCu NPs on the supports and pretreatments (Step 2). More detailed information about the synthesis, characterization and catalytic tests are included as Supporting Information (SI, section 1).

Briefly, the Au-seeds and AuCu colloidal NPs were synthesized by adapting the protocols described by Peng et al.63 and Najafishirtari et al.25, respectively. After purification, AuCu NPs were analyzed by X-ray diffraction (XRD), Transmission Electron Microscopy (TEM), UV-Vis (ultraviolet-visible) spectroscopy and Inductively Coupled Plasma Optical Emission Spectrometry (ICP-OES), to identify the crystalline structure, size, morphology, and composition. To produce the catalysts, the same batch of AuCu NPs were impregnated on commercial SiO₂ (SBET: 380 m².g⁻¹) and CeO₂ (SBET: 60 m².g⁻¹), with metal loading around 3 % (w/w). 500 mg of the support was added to a round-bottom flask containing hexane. The mixture was magnetically stirred for 5 min, ultrasonicated for 10 min and stirred again for more 5 min. After that, 6 mL of colloidal NPs were slowly dropped, and the mixture was magnetically stirred for 1h. The hexane was removed under vacuum and the solid was dried at 70 °C during 1h. The as-prepared samples (fresh catalysts) were labeled as AuCu SiO₂ and AuCu CeO₂, respectively. The catalysts were characterized by XRD, TEM/STEM/EDS (STEM - scanning transmission electron microscopy; EDS - energy dispersed spectroscopy), and ICP-OES. Besides, the catalysts were analyzed by in situ XAFS, at Au-L₃ and Cu-K edges, and by in situ XRD using the facilities at the Brazilian Synchrotron Light Laboratory, LNLS. The protocol used for these experiments is presented in Figure S1.

For CO-PROX reaction, 50 mg of catalyst were diluted with the ground quartz, 100 Mesh (catalyst:quartz 1:3 w/w) and placed in a quartz fixed bed tubular reactor. The reaction was carried out with 1 % CO, 1 % O₂, 70 % H₂ and He for balance, with a total flow of 100 mL.min⁻¹. The reaction was carried out from room temperature (~30 °C) up to 300 °C, with a rate of 2 °C.min⁻¹. The CO conversion was measured using a 7890A Gas Chromatograph (Agilent Technologies) with a TCD detector. Three catalytic cycles were carried out with calcined,

reduced and oxidized catalyst, respectively. The stability of the catalysts was evaluated at 200 °C after these cycles. Figure S2 shows the detailed protocol of the CO-PROX reaction.



Schema 1. Protocol for catalyst preparation. Step 1: colloidal synthesis of AuCu NPs by the two-pot approach. Step 2: wet impregnation of purified AuCu NPs on SiO₂ and CeO₂ supports, producing fresh AuCu_SiO₂ and AuCu_CeO₂ catalysts, respectively. The catalysts were submitted to different pretreatments and used in the CO-PROX reaction.

3. Results and discussion

3.1 Characterization of the AuCu NPs and the AuCu-based catalysts

AuCu NPs were synthesized by a two-pot approach using Au-seeds with an average size of 6.2 \pm 1.0 nm (Fig. S3a). During the synthesis, Cu is reduced and incorporated into the Au lattice, forming the AuCu alloy. The final Au:Cu molar ratio obtained by ICP-OES was 1.02 ± 0.06 and

the formation of AuCu nanoalloy NPs was confirmed by UV-Vis spectroscopy, by the red shift of the original Au NPs surface plasmon resonance from 520 nm to 545 nm (Fig. S3b). Au and Cu monometallic NPs present surface plasmon resonance at around 520 and 570 nm, respectively. 64,65 In heterostructures, the bands related to the plasmon resonances of each metal can be identified in the spectra, while in the case of a nanoalloy, an intermediary absorption band is formed 66.

The diffraction pattern of the AuCu NPs (Fig. 1a) matches the tetragonal structure of the AuCu intermetallic (Au_{0.50}Cu_{0.50}), characterized by the peaks at $2\theta = 31.9^{\circ}$, 49.6 and 52.4° (110, 002) and 201 planes, respectively) that appears due to the chemical order. These peaks, however, have attenuated intensity, suggesting the coexistence of random AuCu alloy domains. The final AuCu NPs presented a narrow size distribution with an average size of 6.0 ± 0.5 nm (Fig. 1b). It is interesting to note that the expected diameter of a Au_{0.50}Cu_{0.50} NP derived from a 6.0 nm Au NP is 7.4 nm, considering the 2-fold increase in the number of atoms and the contraction of the lattice parameter. ⁶⁷ Therefore, the final average size of the AuCu NPs suggests that the Au–seeds were partially etched during the synthesis by the presence of Cu²⁺, residual Cl⁻ and dissolved O₂ in the reaction medium, as indicated by the detection of Au on the supernatant by ICP-OES and reports in the literature. 68-70 The modification of the unoccupied projected-density of states identified by X-ray absorption near-edge structure (XANES) at Au-L₃ (Fig. 1c) and Cu-K (Fig. 1d) edges (dark red lines) is in agreement with the formation of an AuCu alloy. 71 The increase of the absorption intensity around 11930 eV in the Au-L₃ XANES spectrum is originated in the charge transfer of d electrons from Au to Cu while the increase of the absorption intensity at 8980 eV in Cu-K XANES spectrum corresponds to the transfer of s-p electrons from Cu to Au.²⁸ The electron redistribution leads to charge neutrality and respects the electronegativity of the

elements.⁷¹ This trend was also found by Destro *et al.*³⁴ which followed the synthesis of AuCu NPs by one-pot approach by in situ XAFS.

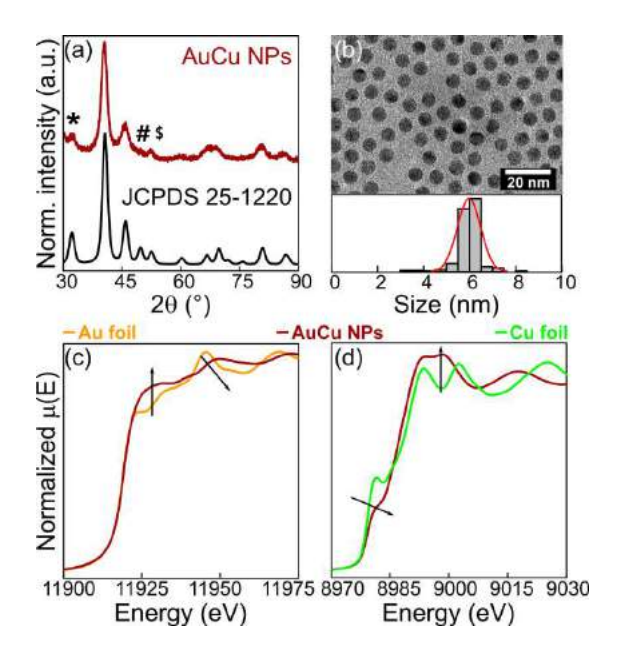


Figure 1. (a) XRD pattern of the AuCu NPs (dark red line) compared with ordered tetragonal AuCu phase (black line, JCPDS 25-1220); *, # and \$ indicate, respectively, 110, 002 and 201 reflections, related to the chemically ordered AuCu alloy; (b) TEM image of the AuCu NPs and the corresponding histogram of size distribution, scale bar: 20 nm.; (c,d) XANES spectra of the AuCu colloidal NPs at Au-L₃ and Cu-K edges, respectively. The black arrows indicate the direction of the changes in absorption intensity compared to the monometallic standards.

Extended X-ray Absorption Fine Structure (EXAFS) data (Fig. S4, S5 and Tables S1, S2) are consistent with the formation of an AuCu alloy. However, the shorter Cu-Cu bond length ($R_{\text{Cu-Cu}}$ of AuCu NPs = 2.60 Å; expected $R_{\text{Cu-Cu}}$ for ordered AuCu alloy = 2.80 Å) and the presence of a Cu-O scattering contribution indicates a Cu-enriched surface, partially oxidized. The presence of a Cu-enriched surface could be related to the exposure to air and the synthesis method, in which

the Cu diffuses into the pre-formed Au lattice.⁷² Therefore, taking together the TEM, XRD, and EXAFS data, the results indicate that the 6.0 nm AuCu NPs consist of an ordered alloy core and a Cu-enriched random alloy surface, partially oxidized by the contact with air. This partial oxidation and enrichment of the second metal at the surface was also found in other Au-based alloys and is driven by the high electronegativity of the Au.^{24,27,73}

The AuCu NPs were impregnated on SiO₂ and CeO₂, with metal loading of ~2.8 % w/w confirmed by ICP-OES. The fresh catalysts (as-prepared) were analyzed by XRD and HAADF-STEM just after the preparation and compared to the colloidal AuCu NPs (Figure S6). No agglomeration was detected and the minor shift of the XRD peaks to smaller angles compared to the colloidal AuCu NPs were associated with slight oxidation and segregation of Cu by air exposure and interaction with the supports. We found that while no apparent modifications occurred in the fresh AuCu_SiO₂ with storage time at room temperature, the dealloy process progresses in the fresh AuCu_CeO₂, detected by the significant shift of the (111) XRD peak to lower angle after about 2 weeks (Fig. 2a,b, estimated composition base on Vegard's Law for a random fcc AuCu alloy⁶⁷ of Au_{0.90}Cu_{0.10}). Zhang *et al.*¹⁹ reported theoretical calculations of Au-X/CeO₂ (X = Ag, Cu, Pd, Pt, Rh, and Ru) in which they confirmed that some metals prefer to bind to CeO₂ than to Au and spontaneously segregate, which was the case of Cu. Other reports in literature also mention the charge transfer from Cu⁰ to CeO₂, resulting in the reduction of Ce⁴⁺ to Ce³⁺ and oxidation of the metal.^{74,75}

The fresh catalysts were submitted to calcination under synthetic air and analyzed by in situ XRD (Fig. 2 a,b). This step is performed to remove the organic ligands that cap the NPs and is particularly important for catalytic applications, to expose the active sites to the reactants.³²

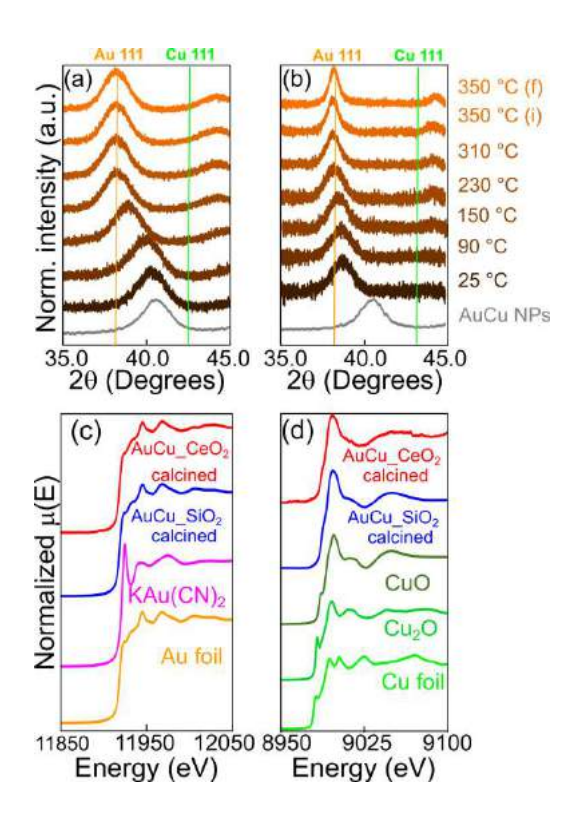


Figure 2. (a, b) In situ XRD patterns of fresh* (a) AuCu_SiO₂ and (b) AuCu_CeO₂ collected during calcination. The gray lines indicate the XRD pattern of the colloidal AuCu NPs. The degree from black to orange indicates the increase in temperature. The vertical yellow and green lines indicate the position of the (111) peak of Au (2θ = 38.2° - JCPDS 04-0784) and Cu (2θ = 43.3° - JCPDS 04-0836), respectively. (c,d) XANES spectra of AuCu_SiO₂ (blue lines) and AuCu_CeO₂ (red lines) after calcination and standards: (c) Au-L₃ and (d) Cu-K edges.* storage time for about 2 weeks.

During the heating process, both materials presented a progressive shift of the (111) peak to lower angles up to 230 °C. The final peak position for both materials was $2\theta = 38.2^{\circ}$, corresponding to the fcc Au lattice parameter (a = 4.08 Å). The complete AuCu dealloy was

corroborated by XAFS data. XANES spectra after calcination at Au-L₃ edge (Fig. 2c) matched the Au foil standard, while the EXAFS data analysis gave an Au-Au bond length of 2.85 Å, close to the Au bulk one (2.88 Å), see Figs. S4, S5 and Table S1. At Cu-K edge (Fig. 2d), the final XANES spectra are comparable to the CuO standard, and EXAFS revealed the presence of Cu-O and Cu-Cu scattering paths, indicating the presence of partially ordered CuO_x species for both materials (Figs. S4, S5 and Table S2).

The main difference among the XRD patterns during the calcination is the evolution of the full width at half maximum (FWHM) from 230 up to 350 °C. After the complete dealloy, that occurred at ~ 230 °C, the FWHM of Au NPs supported on SiO₂ presented subtle changes, whereas the CeO₂-supported NPs decreased. Ex situ XRD patterns obtained for the catalysts calcined at the laboratory (Fig. S6a,b) were more similar and suggest that the temperature reached during the in situ experiments were higher. By TEM analysis (Fig. 3), the average sizes of AuCu SiO₂ (Fig. 3a) and AuCu CeO₂ (Fig. 3b) catalysts calcined at the laboratory were $6.0 \pm$ 1.1 and 6.6 ± 1.8 nm, respectively. The main difference is a slightly broader size distribution in the case of the AuCu CeO₂ catalyst, with Au NPs in the size range of 3 to 11 nm (Fig. 3 b). These results indicate that the AuCu NPs on CeO₂ were more prone to sinter under similar calcination conditions. While it has been demonstrated that a strong interaction between Au NPs and CeO₂ enhances their stability against sintering⁴⁵, in the case of AuCu alloy NPs, it has been shown that the formation of Au-CuO_x-SiO₂ interface during calcination improves the NPs sintering resistance on SiO₂. 19,27,76-78 EDS analysis (Figs. 3 and S7) showed that the dispersion of CuO_x species was dependent on the support; while on SiO₂, the CuO_x species remain in the vicinity of the Au NPs, on CeO₂ the CuO_x species migrate away from the Au NPs spreading on

the support surface, comparable to the effect found in Al₂O₃ surface.^{25,30} These results may explain the differences in the final size distribution of Au NPs after calcination.

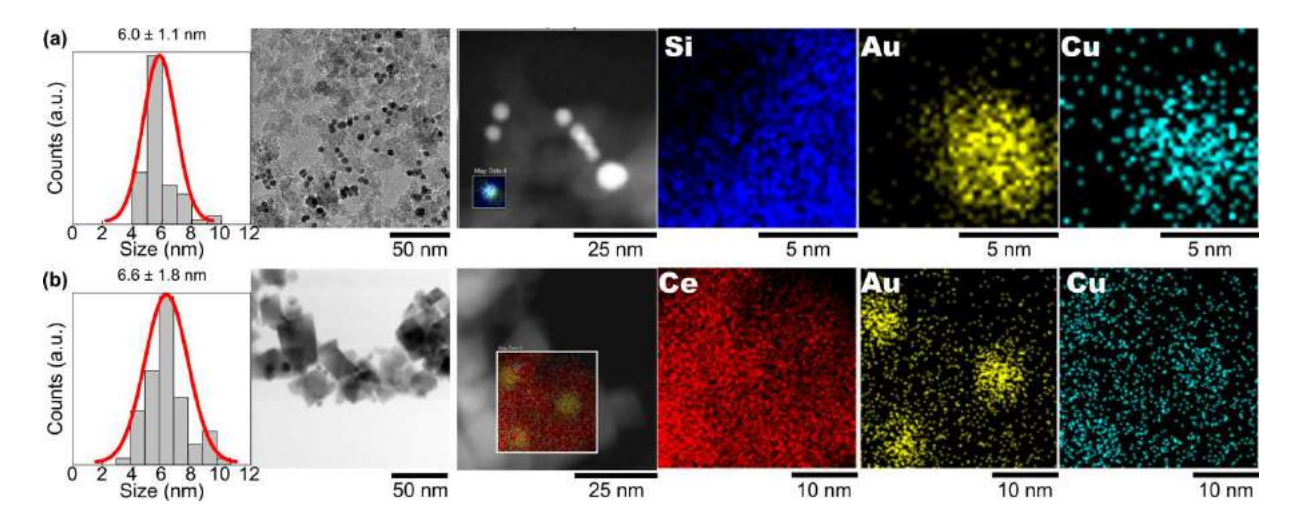


Figure 3. Size distribution histograms, TEM images, and EDS maps of calcined (a) AuCu_SiO₂ and (b) AuCu_CeO₂. Blue, red, yellow and cyan indicate, respectively, Si, Ce, Au and Cu signals. Scale bars are indicated in each image.

After the calcination, both catalysts were analyzed under redox conditions, by alternating oxidative and reductive atmospheres, to better understand the reversibility of dealloy/realloy process (Fig. 4). The realloy process takes place by the reincorporation of Cu into the Au NPs, shifting the peak positions toward higher angles. Under the H₂ atmosphere (pink lines), this takes place at 300 °C for AuCu_SiO₂ (Fig. 4a) and at 200 °C for AuCu_CeO₂ (Fig. 4b). The impact of the Cu-CeO₂ interaction in the reducibility of CuO is widely discussed in literature.^{79–81} For example, Lykaki *et al.*⁸¹ reported that the Cu²⁺ is reduced to Cu⁰ at a lower temperature when CuO is supported on CeO₂, in comparison with bare CuO and the morphology of the CeO₂ particles affected the reducibility of CuO. On the other hand, the Cu-CeO₂ interaction also

impacts on the reducibility of CeO₂, which presents a lower temperature of reduction in the presence of Cu (even for small amounts).⁸²

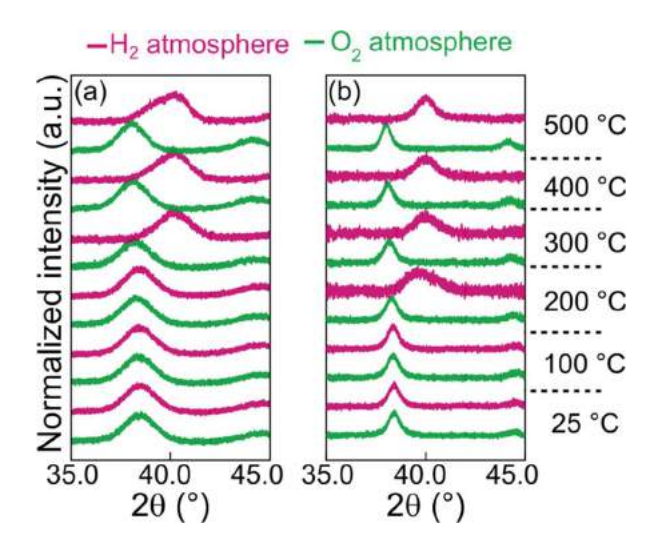


Figure 4. In situ XRD of (a) AuCu_SiO₂ and (b) AuCu_CeO₂ during the redox cycles from room temperature up to 500 °C, alternating synthetic air (green lines) and H₂ flows (pink lines).

The in situ XRD and XANES during reductive pretreatment (Fig. 5 a-d) showed that the realloy process occurs gradually up to 400 °C. The AuCu_CeO₂ catalyst (Fig. 5 b,d) presented Cu reincorporation at a lower temperature than AuCu_SiO₂ (Fig. 5 a,c), as expected based on the in situ XRD redox cycles (Figure 4). EXAFS of the AuCu_SiO₂ catalyst after reduction shows, however, that a small contribution of Cu-O scattering remains at the end of the reduction process (Figs. S4, S5 and Table S2). Unfortunately, it was not possible to obtain satisfactory EXAFS data of the AuCu_CeO₂ catalyst to confirm whether a residual Cu-O contribution remained in this catalyst after the reductive pre-treatment. Nevertheless, it is important to remark that the in situ experiments showed (Figures 2, 4 and 5) that although CeO₂ favored the AuCu dealloy

process and formation of CuO_x species under oxidizing conditions at lower temperature than SiO_2 , it also favored the reduction and Cu reincorporation into the Au lattice at lower temperatures when the catalysts were exposed to reducing conditions. This effect could be expected due to the oxygen storage capacity of CeO_2 and it was nicely demonstrated by these in situ measurements.

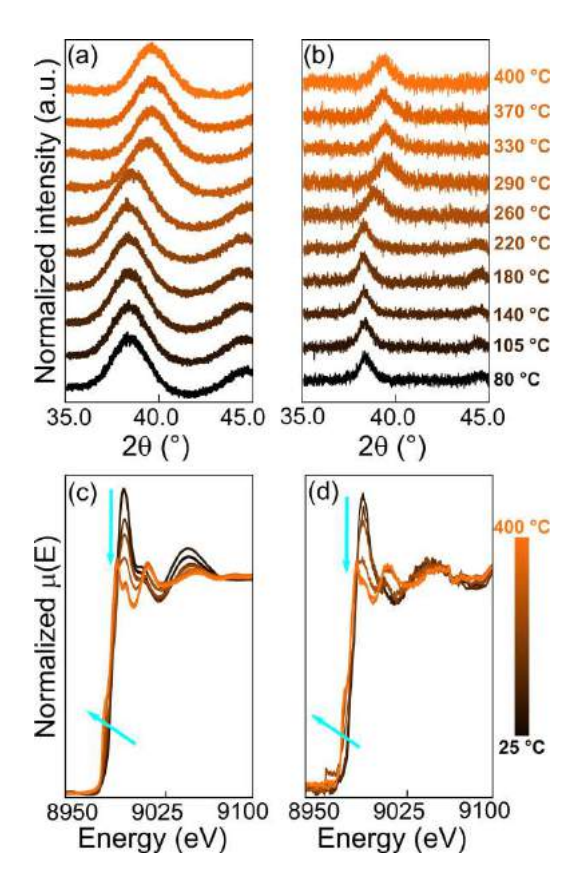
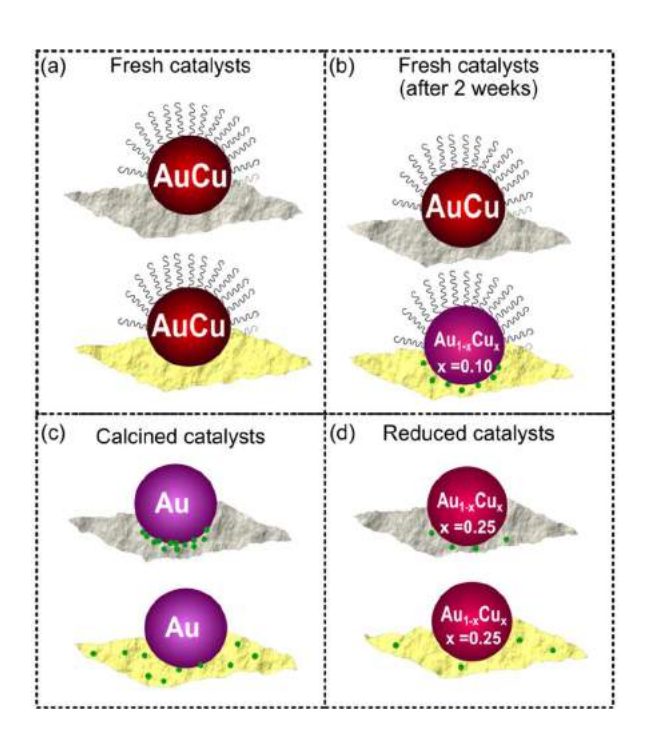


Figure 5. In situ XRD of (a) AuCu_SiO₂ and (b) AuCu_CeO₂ during the reductive pretreatment under H₂ flow from 80 °C (black line) up to 400 °C (orange line). In situ XANES at Cu-K edge of (c) AuCu_SiO₂ and (d) AuCu_CeO₂ during the reductive pretreatment under H₂ flow from 25 °C (black line) up to 400 °C (orange line); the cyan arrows indicate the evolution of the absorption intensity as a function of temperature.

The composition of AuCu_SiO₂ and AuCu_CeO₂ catalysts after the reductive pretreatment was Au_{0.75}Cu_{0.25} for both catalysts. The Cu contents in both catalysts were around two times higher than those found for 14 nm AuCu NPs supported on SiO₂ submitted to similar conditions and more homogeneous when compared to AuCu/Al₂O₃ catalyst.³⁰ The main reason for this difference is likely the size of the AuCu NPs since smaller NPs should facilitate the Cu diffusion into the Au lattice. Based on the in situ XRD and XAFS results, we established the H₂ reduction at 400 °C to induce in situ the Au_{1-x}Cu_x realloy, leading to similar Cu content in both catalysts. It is worth to note that the catalytic reactions took place at lower temperatures. EDS mapping confirmed that Cu is found in the same region as Au after reduction, corroborating the realloy process shown by in situ XRD and XANES experiments (Figure S8). Schema 2 summarizes the evolution of the catalysts under different pretreatments.



Schema 2. Evolution of the catalysts: (a) as-prepared AuCu NPs supported on SiO₂ (gray) and CeO₂ (yellow). The black wavy lines indicate the organic ligands on the AuCu NPs surface. (b) AuCu NPs go through spontaneous dealloy once supported on CeO₂ at room temperature, forming Au_{0.90}Cu_{0.10} and CuO_x (tiny green spheres) on the support surface, while no modification takes place in the fresh AuCu_SiO₂ catalyst. (c) During calcination, the organic ligands are removed and both catalysts are formed by Au NPs and CuO_x species in contact with the support; these CuO_x species remain in the vicinity of the Au NPs on SiO₂ and spread on the CeO₂ surface. (d) After reductive pretreatment, a partial realloy process takes place leading to the final composition of Au_{0.75}Cu_{0.25}.

3.2 Catalytic activity

The catalytic performance of AuCu_SiO₂ and AuCu_CeO₂ catalysts in the CO-PROX reaction are shown in Fig. 6 and Table 1. During the heating step, the calcined AuCu_SiO₂ catalyst presented maximum CO conversion (MC) lower than 20 % at 291 °C (temperature of MC, TMC) (Fig. 6a, 1st cycle). The O₂ conversion, however, achieved 100 % conversion, indicating the high consumption of this reactant by parallel reactions, such as H₂ oxidation. During the cooling process, the activity of AuCu_SiO₂ increased, achieving an MC of 42 % at a much lower temperature (TMC = 214 °C). Cu sites in the AuCu alloy are known to activate the reactional species in PROX-CO reaction and the highly reductive atmosphere of this reaction could promote the formation of Au_{1-x}Cu_x alloy at the end of the heating step. Both bare SiO₂ and CeO₂ have a low catalytic activity to CO-PROX up to 300 °C. ^{83,84}.

The comparison of the performance of AuCu SiO₂ with the monometallic catalysts confirmed that the AuCu alloy is more active than isolated Au or Cu (Fig. S9). The in situ XRD data showed that 300 °C was enough to favor the realloy process for AuCu SiO₂, under diluted H₂. Therefore, it is plausible to associate the increase of activity during the cooling step to the reduction of CuO_x species that could block the most active sites and in situ formation of Au₁-_xCu_x. However, the higher activity achieved below 100 °C indicated that the reductive pretreatment favored the reincorporation of higher contents of Cu compared to the soak time at 300 °C under CO-PROX atmosphere. This was confirmed by the similar reaction profile obtained after reductive pretreatment (Fig. 6a, 2nd cycle; reduced AuCu SiO₂ catalyst). After the 2nd cycle, the catalyst was oxidized and a 3rd catalytic test was carried out (Fig. 6a, 3rd cycle). The catalytic activity significantly decreased, presenting an overall behavior similar to the calcined sample. These results clearly showed the reversibility of the dealloy/realloy process and the better catalytic activity of Au_{1-x}Cu_x alloy in comparison with Au-CuO_x species when supported on SiO₂. This is in agreement with the work by Liu et al.⁵⁸, that reported that the catalytic performance of AuCu supported on silica gel was dependent on the Au:Cu ratio, but in all cases, the AuCu was more active than the monometallic counterparts.

Table 1 – Maximum CO conversion % (MC) and temperature of MC (TMC) of AuCu_SiO₂ and AuCu_CeO₂ during heating and cooling steps under CO-PROX reaction.

Catalyst —	Heating		Cooling	
	MC (%)	TMC (°C)	MC (%)	TMC (°C)
AuCu_SiO ₂ calcined	18	291	42	214
AuCu_SiO2 reduced	43	213	48	197
AuCu_SiO2 oxidized	24	250	41	210
AuCu_CeO2	74	210	75	205

calcined				
AuCu_CeO ₂ reduced	73	220	74	200
AuCu_CeO ₂ oxidized	76	210	74	207

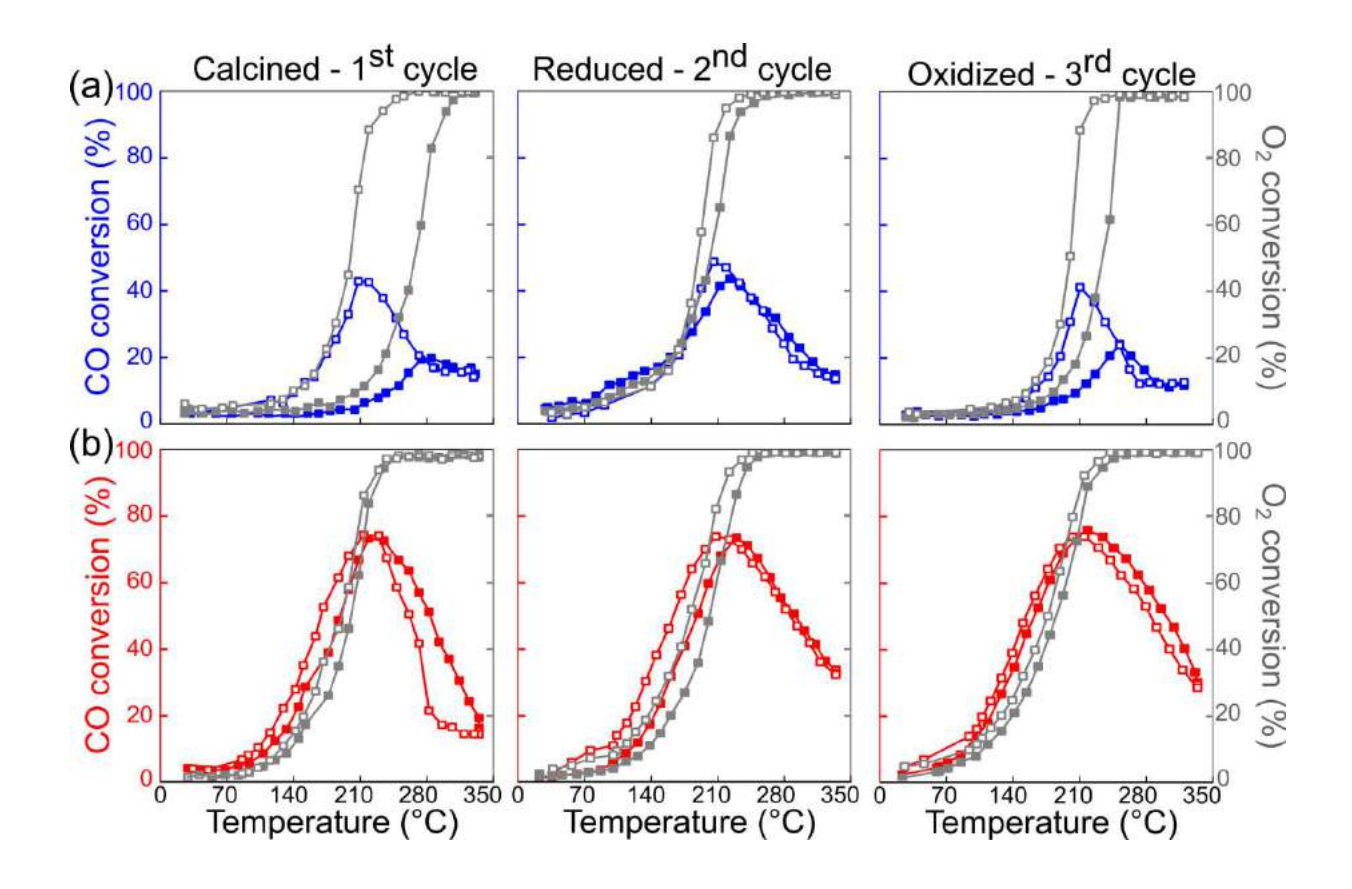


Figure 6. CO conversion (blue and red lines) and O₂ conversion (gray lines) of (a) AuCu_SiO₂ and (b) AuCu_CeO₂ catalysts in CO-PROX reaction. Filled and empty symbols indicate, respectively, heating and cooling processes. Reaction conditions: 1 % CO, 1 % O₂, 70 % H₂, He balance, total flow: 100 mL.min⁻¹, from room temperature up to 300 °C, heating rate: 2 °C.min⁻¹.

Under the same CO-PROX conditions, the AuCu CeO₂ catalyst was always more active than the AuCu SiO₂ catalyst (Fig. 6b and Table 1), with MC of about 75 %. Considering a similar conversion of about 50%, it was achieved at 197 °C for the AuCu SiO2 catalyst under the best condition (during cooling after reduction) and of 165 °C for the AuCu CeO₂ catalyst. Although the increase of the particle size is associated with catalyst deactivation, the AuCu CeO₂ catalyst was more active than the AuCu SiO₂, showing that the participation of the support on the activation of reactional species can offset the slightly larger particle sizes. More interesting, in the case of the AuCu CeO2 catalyst, however, the reductive and oxidative pretreatments had no impact on the performance. The comparison with the monometallic catalysts sheds more light on these results. Figure S10a shows that the Au_CeO2 has similar activity compared to AuCu CeO2 below TMC. Above it, the Au CeO2 became less selective to CO₂ with temperature. Since the Au and AuCu NPs have roughly similar sizes these results showed than on CeO₂, the main impact of Cu insertion in the Au lattice was to improve the selectivity toward CO2 at high temperature, in agreement with the decrease of CO/H surface coverage on Au at high temperature.⁵³ In comparison, Figure S10b shows that the Cu CeO₂ catalyst was much less active under similar conditions. We also evaluated the catalytic activity of the Au CeO₂ catalyst in "poor H₂" CO-PROX conditions (1 % CO, 1 % O₂, 15 % H₂, and He balance), see Figure S11. It can be seen that the oxidized AuCu CeO₂ catalyst responded similarly at low temperatures, independently to the H₂ concentration in the feed (15 or 70%). There was, however, a significant increase in the TMC from 210 °C to 252 °C by decreasing the H₂ that agrees with the competitive adsorption of CO and H₂ on the metallic surface. These results, combined with the in situ experiments that showed that AuCu alloy was stabilized on CeO₂ under reduction conditions, strongly indicate that under CO-PROX the AuCu is stabilized

(see the CO conversion of Au_CeO₂ and AuCu_CeO₂ above TMC in Fig. S10). However, AuCu_CeO₂ and Au_CeO₂ showed similar activities at low temperatures (below TMC) corroborating the important participation of the CeO₂ on the reaction mechanism.

Comparing again the impact of the supports, besides the higher activity, the AuCu_CeO₂ was also more selective than AuCu_SiO₂ (Fig. S12). Nevertheless, it is important to note that S_{CO2} decreased at higher temperatures in both cases due to the excessive consumption of O₂ by parallel reactions, in agreement with previous results.⁸⁵ Looking in more detail, the CO:O₂ conversion ratios can be used as an indicator of the economic viability of a catalyst.⁸⁴ Points between the stoichiometric 2:1 ratio of CO:O₂ and upper limit of 1:1 indicate the predominance of CO oxidation against parallel reactions such as methanation (high CO conversion with low O₂ conversion) or H₂ oxidation (low CO conversion with high O₂ conversion). The AuCu_SiO₂ catalyst presented, in all cycles, most of the points below the upper limit, indicating low selectivity to CO₂ and enhancement of H₂ oxidation. The AuCu_CeO₂, on the other hand, presented points between the two limits up to 200 °C, close to the maximum conversion (Fig. S13).

Stability tests were carried out at 200 °C for the reduced catalysts (Fig. 7). While the AuCu_CeO₂ (Fig 7a, red line) did not deactivate during the stability test, the AuCu_SiO₂ catalyst presented a gradual decrease of CO conversion with time on stream (Fig 7a, blue line). After 7 h, the CO conversion decreased from 40 % to 33 % in the case of AuCu_SiO₂. In general, the deactivation of catalysts is associated with the presence of carbonates and/or coke, due to the sintering of metallic NPs or structural changes of catalytic sites. We did not identify other products besides CO₂ and the carbon balance was close to 100 % (small differences only related to the fluctuations in the baseline), indicating coke and/or carbonates were not the origin of

deactivation. The formation of coke is not expected in Au and Cu catalysts in this reaction but carbonates are known to be formed extensively on the CeO₂ surface and can, in fact, contribute to catalyst deactivation, as in the case of CuO_x/CeO₂ catalysts.⁵⁰ The similar catalytic activity of the AuCu_CeO₂ catalyst between cycles and its higher stability compared to the AuCu_SiO₂ one indicate that extensive carbon deposition was not a crucial issue in this system.

To shed light on the deactivation mechanism of AuCu SiO₂ we modified the protocol of stability test. First, we oxidized the AuCu SiO₂ and performed a new stability test at 200 °C (Fig. S14). The initial CO conversion decreased to 19 % due to Cu oxidation, but no significant deactivation was detected. This result suggests that the Au_{1-x}Cu_x alloy in the reduced AuCu SiO₂ catalyst was gradually oxidized under CO-PROX reaction conditions, decreasing the activity reaching the condition observed for the oxidized catalyst. To confirm this interpretation, we reduced again the AuCu SiO₂ catalyst and cycle the temperature: the temperature was increased to 300 °C under reaction conditions for 30 min and decreased to 20 °C and this cycle was performed twice (Fig. 7b). The catalytic activity increased to about 40 % after exposing the catalysts at 300 °C, the same value obtained after the reductive pretreatment. However, the deactivation pattern was resumed at 200 °C. These results corroborate that the deactivation was caused by the oxidation of Cu⁰ by the O₂ at 200 °C, and the catalytic activity can be recovered by Cu reincorporation forming the Au_{1-x}Cu_x alloy by heating at 300 °C. They also agree with the in situ XRD data (Fig. 4a, 5a), which showed that Au_{1-x}Cu_x alloy is formed at a higher temperature in AuCu_SiO₂ compared to AuCu_CeO₂. We can conclude, therefore, that the temperature employed in the stability test was enough to prevent Cu oxidation in AuCu CeO2 but not on AuCu SiO₂, making AuCu CeO₂ stable under the tested conditions.

It is worth to mention that a slight increase in the average size of the metallic NPs in $AuCu_SiO_2$ (Fig 7 c,d) after the stability tests occurred, as shown in Fig. 7b. We associate this change with a faster deactivation rate compared to the original test (Figure 7a). Cu diffusion into the Au lattice is more difficult in larger NPs and likely leads to higher Cu-enrichment on the surface compared with the initial NPs. The higher Cu-enrichment would favor the oxidation of the Cu and deactivation under the reaction conditions of the $AuCu_SiO_2$ catalyst. The $AuCu_CeO_2$ also presented a similar increase in the average particle size (7.6 \pm 2.6 nm) but considering that this support favors the stabilization of the $Au_{1-x}Cu_x$ alloy on the surface, deactivation was not observed (data not shown).

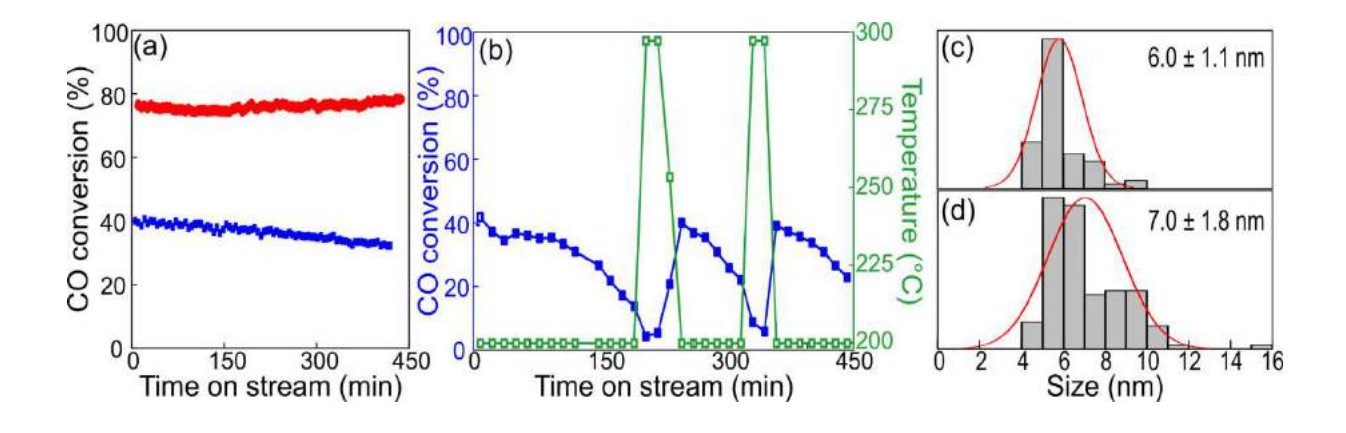


Figure 7. Stability test under CO-PROX condition. (a) CO conversion (%) of AuCu_SiO₂ (blue filled symbols) and AuCu_CeO₂ (red filled symbols). (b) Variation of CO conversion (%) for AuCu_SiO₂ (blue curve) as a function of time and temperature (two heating cycles, from 200 °C up to 300 °C and down to 200 °C under CO-PROX, green curve). Size distributions of the AuCu NPs in the AuCu_SiO₂ catalyst (c) before the catalytic tests (just calcined) and (d) after the catalytic tests. Reaction conditions: 1 % CO, 1 % O₂, 70 % H₂, He balance, total flow: 100 mL.min⁻¹.

The catalytic cycles and stability tests in the CO-PROX reaction clearly indicates the impact of CeO₂ on the catalytic performance in comparison with the SiO₂-supported AuCu NPs. The CeO₂ has an important role not only in providing oxygen from its lattice to oxidize the CO to CO₂ at a lower temperature but also in stabilizing the more active species on the catalyst surface. Although we were not able to perform in situ measurements of our catalyst under CO-PROX condition due to the setup limitation in using pure H₂, the redox cycles and reducing experiments followed by in situ XANES and XRD probed the evolution of the oxidation state and structural properties of the AuCu alloy in contact with SiO₂ or CeO₂ under oxidizing and reducing conditions. The easier oxidation of Cu and dealloying from the AuCu NPs in contact with the CeO₂ under an oxidative atmosphere and Cu reduction and realloy at a lower temperature probed the indirect but important effect of the CeO₂ as support in bimetallic catalysts.

4. Conclusion

Bimetallic catalysts can lead to the formation of unique catalytic sites that depends on several parameters. Here, we explored the AuCu-based catalysts, using pre-formed AuCu NPs, to probe the impact of the support, pretreatments and reaction conditions under CO-PROX. More specifically, AuCu NPs with narrow size distribution (6.0 ± 0.5 nm, i.e., $\sigma < 10\%$) allowed us clearly probing the stability and evolution of these bimetallic NPs in contact with SiO₂ (non-reducible) and CeO₂ (reducible) supports when submitted to similar conditions. This strategy hindered the nucleation of monometallic NPs and minimized the initial presence of atomically disperse species which are common by other preparation methods and could significantly affect the catalytic results. In situ measurements and redox cycles associated with the catalytic tests helped to get a clearer picture of the influence of different atmospheres in the changes of the

AuCu alloy NPs depending on the support and their correlation with the catalytic performance. After the calcination process, isolated Au NPs and CuO_x species on both SiO₂ and CeO₂ were formed, but after reduction or exposure to the CO-PROX atmosphere at high temperatures, a partial realloy took place leading to Au-enriched AuCu alloy NPs and Cu species interacting with CeO₂ or SiO₂. In the case of SiO₂, these residual Cu species stayed in the vicinity of the AuCu NPs whereas in the case of CeO₂ they spread on the support. We clearly showed that the Au_{1-x}Cu_x nanoalloy provides the active sites for CO-PROX and that CeO₂ support stabilizes this phase under the reducing conditions of this reaction. In fact, under the oxidative atmosphere, CeO₂ favored a partial dealloy of AuCu NPs even at room temperature. A similar process only took place at high temperatures in the case of SiO₂ support. On the other hand, under reducing conditions, Cu reduction and realloy took place at a lower temperature in the case of CeO₂. The stabilization of the Au_{1-x}Cu_x alloy in AuCu CeO₂ under CO-PROX improved the activity and stability of the catalyst in comparison to the non-reductive SiO₂ support. Although the protocol we used in this work does not have a direct correlation to the catalyst pretreatments that take place at the industrial scale, this simpler approach is general and provided fundamental insights that could be extended to other reactions than CO-PROX.

Acknowledgments

This study was financed in part by the Coordenação de Aperfeiçoamento de Pessoal de Nível Superior - Brazil (CAPES) - Finance Code 001. The authors acknowledge FAPESP (2011/50727-9, 2018/01258-5) for financial support. T.E.R.F. acknowledges the National Council for Scientific and Technological Development (CNPq, 140414/2016-9) for fellowship. D.Z. acknowledges CNPq for financial support (309412/2018-8). The authors thank LNNano for

the access to the JEOL JEM-2100F microscope and LNLS for the access to the XPD and XAFS2 beamlines. Finally, the authors thank D. S. Gonçalves, T.M. Kokumai and I. B. Aragão for their help during the XANES/EXAFS and in situ XRD data collection at LNLS.

References

- (1) Zhang, H.; Jin, M.; Xiong, Y.; Lim, B.; Xia, Y. Shape-Controlled Synthesis of Pd Nanocrystals and Their Catalytic Applications. *Acc. Chem. Res.* **2013**, *46* (8), 1783–1794. https://doi.org/10.1021/ar300209w.
- (2) Janssens, T. V. W.; Clausen, B. S.; Hvolbæk, B.; Falsig, H.; Christensen, C. H.; Bligaard, T.; Nørskov, J. K. Insights into the Reactivity of Supported Au Nanoparticles: Combining Theory and Experiments. *Top. Catal.* **2007**, *44* (1–2), 15–26. https://doi.org/10.1007/s11244-007-0335-3.
- (3) Lentz, C.; Jand, S. P.; Melke, J.; Roth, C.; Kaghazchi, P. DRIFTS Study of CO Adsorption on Pt Nanoparticles Supported by DFT Calculations. *J. Mol. Catal. A Chem.* **2017**, *426*, 1–9. https://doi.org/10.1016/j.molcata.2016.10.002.
- (4) Hvolbæk, B.; Janssens, T. V. W.; Clausen, B. S.; Falsig, H.; Christensen, C. H.; Nørskov, J. K. Catalytic Activity of Au Nanoparticles. *Nano Today* **2007**, *2* (4), 14–18. https://doi.org/10.1016/S1748-0132(07)70113-5.
- (5) Shekhar, M.; Wang, J.; Lee, W.-S.; Williams, W. D.; Kim, S. M.; Stach, E. A.; Miller, J. T.; Delgass, W. N.; Ribeiro, F. H. Size and Support Effects for the Water–Gas Shift Catalysis over Gold Nanoparticles Supported on Model Al₂O₃ and TiO₂. *J. Am. Chem. Soc.* **2012**, *134* (10), 4700–4708. https://doi.org/10.1021/ja210083d.
- (6) Wu, J.; Qi, L.; You, H.; Gross, A.; Li, J.; Yang, H. Icosahedral Platinum Alloy Nanocrystals with Enhanced Electrocatalytic Activities. *J. Am. Chem. Soc.* **2012**, *134* (29), 11880–11883. https://doi.org/10.1021/ja303950v.
- (7) Li, J.; Chen, W.; Zhao, H.; Zheng, X.; Wu, L.; Pan, H.; Zhu, J.; Chen, Y.; Lu, J. Size-Dependent Catalytic Activity over Carbon-Supported Palladium Nanoparticles in Dehydrogenation of Formic Acid. *J. Catal.* **2017**, *352*, 371–381. https://doi.org/10.1016/j.jcat.2017.06.007.
- (8) Johnston, R. L. Metal Nanoparticles and Nanoalloys. In *Frontiers of Nanoscience*; Johnston, R. L., Wilcoxon, J. P., Eds.; Elsevier, 2012; Vol. 3, pp 1–42. https://doi.org/10.1016/B978-0-08-096357-0.00006-6.
- (9) Ferrando, R.; Jellinek, J.; Johnston, R. L. Nanoalloys: From Theory to Applications of Alloy Clusters and Nanoparticles. *Chem. Rev.* **2008**, *108* (3), 845–910. https://doi.org/10.1021/cr040090g.
- (10) Peng, L.; Ringe, E.; Van Duyne, R. P.; Marks, L. D. Segregation in Bimetallic Nanoparticles. *Phys. Chem. Chem. Phys.* **2015**, *17*, 27940–27951. https://doi.org/10.1039/C5CP01492A.
- (11) Wanjala, B. N.; Luo, J.; Loukrakpam, R.; Fang, B.; Mott, D.; Njoki, P. N.; Engelhard, M.;

- Naslund, H. R.; Wu, J. K.; Wang, L.; et al. Nanoscale Alloying, Phase-Segregation, and Core-Shell Evolution of Gold-Platinum Nanoparticles and Their Electrocatalytic Effect on Oxygen Reduction Reaction. *Chem. Mater.* **2010**, *22* (14), 4282–4294. https://doi.org/10.1021/cm101109e.
- (12) Sachtler, J. W. A.; Somorjai, A. G. Influence of Ensemble Size on CO Chemisorption and Catalytic N-Hexane Conversion by Au-Pt(111) Bimetallic Single-Crystal Surfaces. *J. Catal.* **1983**, *81* (1), 77–94. https://doi.org/10.1016/0021-9517(83)90148-3.
- (13) Gao, F.; Goodman, D. W. Pd–Au Bimetallic Catalysts: Understanding Alloy Effects from Planar Models and (Supported) Nanoparticles. *Chem. Soc. Rev.* **2012**, *41* (24), 8009–8020. https://doi.org/10.1039/c2cs35160a.
- (14) Liu, P.; Nørskov, J. K. Ligand and Ensemble Effects in Adsorption on Alloy Surfaces. *Phys. Chem. Chem. Phys.* **2001**, *3* (17), 3814–3818. https://doi.org/10.1039/b103525h.
- (15) Maroun, F. The Role of Atomic Ensembles in the Reactivity of Bimetallic Electrocatalysts. *Science*. **2001**, 293 (5536), 1811–1814. https://doi.org/10.1126/science.1061696.
- (16) Yuan, D.; Gong, X.; Wu, R. Ensemble Effects on Ethylene Dehydrogenation on PdAu(001) Surfaces Investigated with First-Principles Calculations and Nudged-Elastic-Band Simulations. *Phys. Rev. B* **2007**, *75* (23), 233401. https://doi.org/10.1103/PhysRevB.75.233401.
- (17) Sytwu, K.; Vadai, M.; Dionne, J. A. Bimetallic Nanostructures: Combining Plasmonic and Catalytic Metals for Photocatalysis. *Adv. Phys. X* **2019**, *4* (1), 1619480. https://doi.org/10.1080/23746149.2019.1619480.
- (18) Bligaard, T.; Nørskov, J. K. Ligand Effects in Heterogeneous Catalysis and Electrochemistry. *Electrochim. Acta* **2007**, *52* (18), 5512–5516. https://doi.org/10.1016/j.electacta.2007.02.041.
- (19) Zhang, L.; Kim, H. Y.; Henkelman, G. CO Oxidation at the Au-Cu Interface of Bimetallic Nanoclusters Supported on CeO₂(111). *J. Phys. Chem. Lett.* **2013**, *4* (17), 2943–2947. https://doi.org/10.1021/jz401524d.
- (20) Kim, D.; Resasco, J.; Yu, Y.; Asiri, A. M.; Yang, P. Synergistic Geometric and Electronic Effects for Electrochemical Reduction of Carbon Dioxide Using Gold–Copper Bimetallic Nanoparticles. *Nat. Commun.* **2014**, *5* (1), 4948. https://doi.org/10.1038/ncomms5948.
- (21) Chen, T.; Rodionov, V. O. Controllable Catalysis with Nanoparticles: Bimetallic Alloy Systems and Surface Adsorbates. *ACS Catal.* **2016**, *6* (6), 4025–4033. https://doi.org/10.1021/acscatal.6b00714.
- (22) Guisbiers, G.; Mejia-Rosales, S.; Khanal, S.; Ruiz-Zepeda, F.; Whetten, R. L.; José-Yacaman, M. Gold-Copper Nano-Alloy, "Tumbaga", in the Era of Nano: Phase Diagram and Segregation. *Nano Lett.* **2014**, *14* (11), 6718–6726. https://doi.org/10.1021/nl503584q.
- (23) Wang, A.; Liu, X. Y.; Mou, C.-Y.; Zhang, T. Understanding the Synergistic Effects of Gold Bimetallic Catalysts. *J. Catal.* **2013**, *308*, 258–271. https://doi.org/10.1016/j.jcat.2013.08.023.
- (24) Zhou, S.; Yin, H.; Schwartz, V.; Wu, Z.; Mullins, D.; Eichhorn, B.; Overbury, S. H.; Dai, S. In Situ Phase Separation of NiAu Alloy Nanoparticles for Preparing Highly Active Au/NiO CO Oxidation Catalysts. *ChemPhysChem* 2008, 9 (17), 2475–2479. https://doi.org/10.1002/cphc.200800587.
- (25) Najafishirtari, S.; Brescia, R.; Guardia, P.; Marras, S.; Manna, L.; Colombo, M. Nanoscale Transformations of Alumina-Supported AuCu Ordered Phase Nanocrystals and Their

- Activity in CO Oxidation. *ACS Catal.* **2015**, *5* (4), 2154–2163. https://doi.org/10.1021/cs501923x.
- (26) Li, X.; See, S.; Fang, S.; Teo, J.; Foo, Y. L.; Borgna, A.; Lin, M.; Zhong, Z. Activation and Deactivation of Au–Cu/SBA-15 Catalyst for Preferential Oxidation of CO in H₂-Rich Gas. *ACS Catal.* **2012**, *2*, 360–369. https://doi.org/10.1021/cs200536a.
- (27) Liu, X.; Wang, A.; Li, L.; Zhang, T.; Mou, C.-Y. Y.; Lee, J.-F. F. Structural Changes of Au–Cu Bimetallic Catalysts in CO Oxidation: In Situ XRD, EPR, XANES, and FT-IR Characterizations. *J. Catal.* **2011**, 278 (2), 288–296. https://doi.org/10.1016/j.jcat.2010.12.016.
- (28) Bauer, J. C.; Mullins, D.; Li, M.; Wu, Z.; Payzant, E. A.; Overbury, S. H.; Dai, S. Synthesis of Silica Supported AuCu Nanoparticle Catalysts and the Effects of Pretreatment Conditions for the CO Oxidation Reaction. *Phys. Chem. Chem. Phys.* **2011**, 13 (7), 2571. https://doi.org/10.1039/c0cp01859g.
- (29) Najafishirtari, S.; Kokumai, T. M.; Marras, S.; Destro, P.; Prato, M.; Scarpellini, A.; Brescia, R.; Lak, A.; Pellegrino, T.; Zanchet, D.; et al. Dumbbell-like Au_{0.5}Cu_{0.5}@Fe₃O₄ Nanocrystals: Synthesis, Characterization, and Catalytic Activity in CO Oxidation. *ACS Appl. Mater. Interfaces* **2016**, 8 (42), 28624–28632. https://doi.org/10.1021/acsami.6b09813.
- (30) Destro, P.; Kokumai, T. M.; Scarpellini, A.; Pasquale, L.; Manna, L.; Colombo, M.; Zanchet, D. The Crucial Role of the Support in the Transformations of Bimetallic Nanoparticles and Catalytic Performance. *ACS Catal.* **2018**, 8 (2), 1031–1037. https://doi.org/10.1021/acscatal.7b03685.
- (31) Zhan, W.; Wang, J.; Wang, H.; Zhang, J.; Liu, X.; Zhang, P.; Chi, M.; Guo, Y. Y.; Guo, Y. Y.; Lu, G.; et al. Crystal Structural Effect of AuCu Alloy Nanoparticles on Catalytic CO Oxidation. *J. Am. Chem. Soc.* **2017**, *139* (26), 8846–8854. https://doi.org/10.1021/jacs.7b01784.
- (32) Destro, P.; Marras, S.; Manna, L.; Colombo, M.; Zanchet, D. AuCu Alloy Nanoparticles Supported on SiO₂: Impact of Redox Pretreatments in the Catalyst Performance in CO Oxidation. *Catal. Today* **2017**, *282*, 105–110. https://doi.org/10.1016/j.cattod.2016.08.003.
- (33) Li, W.; Wang, A.; Liu, X.; Zhang, T. Silica-Supported Au-Cu Alloy Nanoparticles as an Efficient Catalyst for Selective Oxidation of Alcohols. *Appl. Catal. A Gen.* **2012**, *433*–*434*, 146–151. https://doi.org/10.1016/j.apcata.2012.05.014.
- (34) Destro, P.; Cantane, D. A.; Meira, D. M.; Honório, G. dos S.; Costa, L. S.; Bueno, J. M. C.; Zanchet, D. Formation of Bimetallic Copper-Gold Alloy Nanoparticles Probed by in Situ X-Ray Absorption Fine Structure Spectroscopy. *Eur. J. Inorg. Chem.* 2018, 2018 (33), 3770–3777. https://doi.org/10.1002/ejic.201800413.
- (35) Zhao, C.; Watt, C.; Kent, P. R.; Overbury, S. H.; Mullins, D. R.; Calaza, F. C.; Savara, A.; Xu, Y. Coupling of Acetaldehyde to Crotonaldehyde on CeO_{2-x} (111): Bifunctional Mechanism and Role of Oxygen Vacancies. *J. Phys. Chem. C* 2019, 123 (13), 8273–8286. https://doi.org/10.1021/acs.jpcc.8b08535.
- (36) Yu, L.; Xi, J. CeO₂ Nanoparticles Improved Pt-Based Catalysts for Direct Alcohol Fuel Cells. *Int. J. Hydrogen Energy* **2012**, *37* (21), 15938–15947. https://doi.org/10.1016/j.ijhydene.2012.08.063.
- (37) Chen, Y.; Wang, H.; Burch, R.; Hardacre, C.; Hu, P. New Insight into Mechanisms in Water-Gas-Shift Reaction on Au/CeO₂(111): A Density Functional Theory and Kinetic

- Study. Faraday Discuss. 2011, 152, 121–133. https://doi.org/10.1039/c1fd00019e.
- (38) Aranifard, S.; Ammal, S. C.; Heyden, A. On the Importance of the Associative Carboxyl Mechanism for the Water-Gas Shift Reaction at Pt/CeO₂ Interface Sites. *J. Phys. Chem. C* **2014**, *118* (12), 6314–6323. https://doi.org/10.1021/jp5000649.
- (39) Cargnello, M.; Doan-Nguyen, V. V. T.; Gordon, T. R.; Diaz, R. E.; Stach, E. a.; Gorte, R. J.; Fornasiero, P.; Murray, C. B. Control of Metal Nanocrystal Size Reveals Metal-Support Interface Role for Ceria Catalysts. *Science.* **2013**, *341* (6147), 771–773. https://doi.org/10.1126/science.1240148.
- (40) Hossain, S. T.; Almesned, Y.; Zhang, K.; Zell, E. T.; Bernard, D. T.; Balaz, S.; Wang, R. Support Structure Effect on CO Oxidation: A Comparative Study on SiO₂ Nanospheres and CeO₂ Nanorods Supported CuO_x Catalysts. *Appl. Surf. Sci.* **2018**, *428*, 598–608. https://doi.org/10.1016/j.apsusc.2017.09.199.
- (41) Campbell, C. T. CHEMISTRY: Oxygen Vacancies and Catalysis on Ceria Surfaces. *Science*. **2005**, *309* (5735), 713–714. https://doi.org/10.1126/science.1113955.
- (42) Carrettin, S.; Concepción, P.; Corma, A.; López Nieto, J. M.; Puntes, V. F. Nanocrystalline CeO₂ Increases the Activity of Au for CO Oxidation by Two Orders of Magnitude. *Angew. Chemie Int. Ed.* **2004**, *43* (19), 2538–2540. https://doi.org/10.1002/anie.200353570.
- (43) Si, R.; Flytzani-Stephanopoulos, M. Shape and Crystal-Plane Effects of Nanoscale Ceria on the Activity of Au-CeO₂ Catalysts for the Water–Gas Shift Reaction. *Angew. Chemie Int. Ed.* **2008**, *47* (15), 2884–2887. https://doi.org/10.1002/anie.200705828.
- (44) Schubert, M. M.; Hackenberg, S.; van Veen, A. C.; Muhler, M.; Plzak, V.; Behm, R. J. CO Oxidation over Supported Gold Catalysts—"Inert" and "Active" Support Materials and Their Role for the Oxygen Supply during Reaction. *J. Catal.* **2001**, *197* (1), 113–122. https://doi.org/10.1006/jcat.2000.3069.
- (45) Ta, N.; Liu, J. (Jimmy); Chenna, S.; Crozier, P. A.; Li, Y.; Chen, A.; Shen, W. Stabilized Gold Nanoparticles on Ceria Nanorods by Strong Interfacial Anchoring. *J. Am. Chem. Soc.* 2012, 134 (51), 20585–20588. https://doi.org/10.1021/ja310341j.
- (46) Liu, W.; Flytzani-Stephanopoulos, M. Transition Metal-Promoted Oxidation Catalysis by Fluorite Oxides: A Study of CO Oxidation over Cu-CeO₂. *Chem. Eng. J. Biochem. Eng. J.* **1996**, *64* (2), 283–294. https://doi.org/10.1016/S0923-0467(96)03135-1.
- (47) Liu, W.; Flytzanistephanopoulos, M. Total Oxidation of Carbon-Monoxide and Methane over Transition Metal Fluorite Oxide Composite Catalysts. *J. Catal.* **1995**, *153* (2), 317–332. https://doi.org/10.1006/jcat.1995.1133.
- (48) Caputo, T.; Lisi, L.; Pirone, R.; Russo, G. On the Role of Redox Properties of CuO/CeO₂ Catalysts in the Preferential Oxidation of CO in H₂-Rich Gases. *Appl. Catal. A Gen.* **2008**, 348 (1), 42–53. https://doi.org/10.1016/j.apcata.2008.06.025.
- (49) Gamarra, D.; Belver, C.; Fernández-García, M.; Martínez-Arias, A. Selective CO Oxidation in Excess H₂ over Copper—Ceria Catalysts: Identification of Active Entities/Species. *J. Am. Chem. Soc.* **2007**, *129* (40), 12064–12065. https://doi.org/10.1021/ja073926g.
- (50) Gamarra, D.; Martínez-Arias, A. Preferential Oxidation of CO in Rich H₂ over CuO/CeO₂: Operando-DRIFTS Analysis of Deactivating Effect of CO₂ and H₂O. *J. Catal.* **2009**, *263* (1), 189–195. https://doi.org/10.1016/j.jcat.2009.02.012.
- (51) Wu, Z.; Zhu, H.; Qin, Z.; Wang, H.; Ding, J.; Huang, L.; Wang, J. CO Preferential Oxidation in H₂-Rich Stream over a CuO/CeO₂ Catalyst with High H₂O and CO₂

- Tolerance. Fuel **2013**, 104, 41–45. https://doi.org/10.1016/j.fuel.2010.03.001.
- (52) Barroso-Martín, I.; Infantes-Molina, A.; Talon, A.; Storaro, L.; Rodríguez-Aguado, E.; Rodríguez-Castellón, E.; Moretti, E. CO Preferential Photo-Oxidation in Excess of Hydrogen in Dark and Simulated Solar Light Irradiation over AuCu-Based Catalysts on SBA-15 Mesoporous Silica-Titania. *Materials (Basel)*. **2018**, *11* (7), 1203. https://doi.org/10.3390/ma11071203.
- (53) Kandoi, S.; Gokhale, A. A.; Grabow, L. C.; Dumesic, J. A.; Mavrikakis, M. Why Au and Cu Are More Selective Than Pt for Preferential Oxidation of CO at Low Temperature. *Catal. Letters* **2004**, *93* (1/2), 93–100. https://doi.org/10.1023/B:CATL.0000016955.66476.44.
- (54) Fiorenza, R.; Crisafulli, C.; Condorelli, G. G.; Lupo, F.; Scirè, S. Au-Ag/CeO₂ and Au-Cu/CeO₂ Catalysts for Volatile Organic Compounds Oxidation and CO Preferential Oxidation. *Catal. Letters* **2015**, *145* (9), 1691–1702. https://doi.org/10.1007/s10562-015-1585-5.
- (55) Jing, G.; Zhang, L.; Ma, Y.; Wu, J.; Wang, Q.; Wu, G.; Yan, L.; Zeng, S. Comparison of Au–Ce and Au–Cu Interaction over Au/CeO₂–CuO Catalysts for Preferential CO Oxidation. *CrystEngComm* **2019**, *21* (2), 363–371. https://doi.org/10.1039/C8CE01839A.
- (56) Laguna, O. H.; Hernández, W. Y.; Arzamendi, G.; Gandía, L. M.; Centeno, M. A.; Odriozola, J. A. Gold Supported on CuO_x/CeO₂ Catalyst for the Purification of Hydrogen by the CO Preferential Oxidation Reaction (PROX). *Fuel* **2014**, *118*, 176–185. https://doi.org/10.1016/j.fuel.2013.10.072.
- (57) Liao, X.; Chu, W.; Dai, X.; Pitchon, V. Bimetallic Au–Cu Supported on Ceria for PROX Reaction: Effects of Cu/Au Atomic Ratios and Thermal Pretreatments. *Appl. Catal. B Environ.* **2013**, *142–143*, 25–37. https://doi.org/10.1016/j.apcatb.2013.05.010.
- (58) Liu, X.; Wang, A.; Zhang, T.; Su, D.-S.; Mou, C.-Y. Au–Cu Alloy Nanoparticles Supported on Silica Gel as Catalyst for CO Oxidation: Effects of Au/Cu Ratios. *Catal. Today* **2011**, *160* (1), 103–108. https://doi.org/10.1016/j.cattod.2010.05.019.
- (59) Potemkin, D. I.; Snytnikov, P. V.; Semitut, E. Y.; Plyusnin, P. E.; Shubin, Y. V.; Sobyanin, V. A. Bimetallic Au-Cu/CeO₂ Catalyst: Synthesis, Structure, and Catalytic Properties in the CO Preferential Oxidation. *Catal. Ind.* **2014**, *6* (1), 36–43. https://doi.org/10.1134/S2070050414010073.
- (60) Fonseca, J. da S. L.; Ferreira, H. S.; Bion, N.; Pirault-Roy, L.; Rangel, M. do C.; Duprez, D.; Epron, F. Cooperative Effect between Copper and Gold on Ceria for CO-PROX Reaction. *Catal. Today* **2012**, *180* (1), 34–41. https://doi.org/10.1016/j.cattod.2011.06.008.
- (61) Lee, H. C.; Kim, D. H. Kinetics of CO and H2 Oxidation over CuO-CeO₂ Catalyst in H₂ Mixtures with CO₂ and H₂O. *Catal. Today* **2008**, *132* (1–4), 109–116. https://doi.org/10.1016/j.cattod.2007.12.028.
- (62) Scirè, S.; Crisafulli, C.; Riccobene, P. M.; Patanè, G.; Pistone, A. Selective Oxidation of CO in H2-Rich Stream over Au/CeO₂ and Cu/CeO₂ Catalysts: An Insight on the Effect of Preparation Method and Catalyst Pretreatment. *Appl. Catal. A Gen.* **2012**, *417–418*, 66–75. https://doi.org/10.1016/j.apcata.2011.12.025.
- (63) Peng, S.; Lee, Y.; Wang, C.; Yin, H.; Dai, S.; Sun, S. A Facile Synthesis of Monodisperse Au Nanoparticles and Their Catalysis of CO Oxidation. *Nano Res.* **2008**, *1* (3), 229–234. https://doi.org/10.1007/s12274-008-8026-3.
- (64) Link, S.; El-Sayed, M. A. Size and Temperature Dependence of the Plasmon Absorption

- of Colloidal Gold Nanoparticles. *J. Phys. Chem. B* **1999**, *103* (21), 4212–4217. https://doi.org/10.1021/jp9847960.
- (65) Dang, T. M. D.; Le, T. T. T.; Fribourg-Blanc, E.; Dang, M. C. Synthesis and Optical Properties of Copper Nanoparticles Prepared by a Chemical Reduction Method. *Adv. Nat. Sci. Nanosci. Nanotechnol.* 2011, 2 (1), 015009. https://doi.org/10.1088/2043-6262/2/1/015009.
- (66) Ristig, S.; Prymak, O.; Loza, K.; Gocyla, M.; Meyer-Zaika, W.; Heggen, M.; Raabe, D.; Epple, M. Nanostructure of Wet-Chemically Prepared, Polymer-Stabilized Silver-Gold Nanoalloys (6 Nm) over the Entire Composition Range. *J. Mater. Chem. B* **2015**, *3* (23), 4654–4662. https://doi.org/10.1039/C5TB00644A.
- (67) Okamoto, H.; Chakrabarti, D. J.; Laughlin, D. E.; Massalski, T. B. The Au-Cu (Gold-Copper) System. *J. Phase Equilibria* **1987**, 8 (5), 454–474. https://doi.org/10.1007/BF02893155.
- (68) Wen, T.; Zhang, H.; Tang, X.; Chu, W.; Liu, W.; Ji, Y.; Hu, Z.; Hou, S.; Hu, X.; Wu, X. Copper Ion Assisted Reshaping and Etching of Gold Nanorods: Mechanism Studies and Applications. *J. Phys. Chem. C* **2013**, *117* (48), 25769–25777. https://doi.org/10.1021/jp407774s.
- (69) Mettela, G.; Kulkarni, G. U. Facet Selective Etching of Au Microcrystallites. *Nano Res.* **2015**, 8 (9), 2925–2934. https://doi.org/10.1007/s12274-015-0797-8.
- (70) Wang, P.; Qi, X.; Zhang, X.; Wang, T.; Li, Y.; Zhang, K.; Zhao, S.; Zhou, J.; Fu, Y. Solvent: A Key in Digestive Ripening for Monodisperse Au Nanoparticles. *Nanoscale Res. Lett.* **2017**, *12* (1), 25. https://doi.org/10.1186/s11671-016-1797-7.
- (71) Kuhn, M.; Sham, T. K. Charge Redistribution and Electronic Behavior in a Series of Au-Cu Alloys. *Phys. Rev. B* **1994**, 49 (3), 1647–1661. https://doi.org/10.1103/PhysRevB.49.1647.
- (72) Chen, W.; Yu, R.; Li, L.; Wang, A.; Peng, Q.; Li, Y. A Seed-Based Diffusion Route to Monodisperse Intermetallic CuAu Nanocrystals. *Angew. Chemie Int. Ed.* **2010**, *49* (16), 2917–2921. https://doi.org/10.1002/anie.200906835.
- (73) Menning, C. A.; Chen, J. G. General Trend for Adsorbate-Induced Segregation of Subsurface Metal Atoms in Bimetallic Surfaces. *J. Chem. Phys.* **2009**, *130* (17), 174709. https://doi.org/10.1063/1.3125926.
- (74) Nolan, M. Charge Transfer and Formation of Reduced Ce³⁺ upon Adsorption of Metal Atoms at the Ceria (110) Surface. *J. Chem. Phys.* **2012**, *136* (13), 134703. https://doi.org/10.1063/1.3697485.
- (75) Chen, S.; Li, L.; Hu, W.; Huang, X.; Li, Q.; Xu, Y.; Zuo, Y.; Li, G. Anchoring High-Concentration Oxygen Vacancies at Interfaces of CeO_{2-x}/Cu toward Enhanced Activity for Preferential CO Oxidation. *ACS Appl. Mater. Interfaces* **2015**, 7 (41), 22999–23007. https://doi.org/10.1021/acsami.5b06302.
- (76) Giannakakis, G.; Trimpalis, A.; Shan, J.; Qi, Z.; Cao, S.; Liu, J.; Ye, J.; Biener, J.; Flytzani-Stephanopoulos, M. NiAu Single Atom Alloys for the Non-Oxidative Dehydrogenation of Ethanol to Acetaldehyde and Hydrogen. *Top. Catal.* **2018**, *61* (5–6), 475–486. https://doi.org/10.1007/s11244-017-0883-0.
- (77) Bauer, J. C.; Veith, G. M.; Allard, L. F.; Oyola, Y.; Overbury, S. H.; Dai, S. Silica-Supported Au–CuO_x Hybrid Nanocrystals as Active and Selective Catalysts for the Formation of Acetaldehyde from the Oxidation of Ethanol. *ACS Catal.* **2012**, *2* (12), 2537–2546. https://doi.org/10.1021/cs300551r.

- (78) Qiao, P.; Xu, S.; Zhang, D.; Li, R.; Zou, S.; Liu, J.; Yi, W.; Li, J.; Fan, J. Sub-10 Nm Au–Pt–Pd Alloy Trimetallic Nanoparticles with a High Oxidation-Resistant Property as Efficient and Durable VOC Oxidation Catalysts. *Chem. Commun.* **2014**, *50* (79), 11713–11716. https://doi.org/10.1039/C4CC04596C.
- (79) Wang, X.; Rodriguez, J. A.; Hanson, J. C.; Gamarra, D.; Martínez-Arias, A.; Fernández-García, M. In Situ Studies of the Active Sites for the Water Gas Shift Reaction over Cu–CeO₂ Catalysts: Complex Interaction between Metallic Copper and Oxygen Vacancies of Ceria. *J. Phys. Chem. B* **2006**, *110* (1), 428–434. https://doi.org/10.1021/jp055467g.
- (80) Wang, X.; Rodriguez, J. A.; Hanson, J. C.; Gamarra, D.; Martínez-Arias, A.; Fernández-García, M. Ceria-Based Catalysts for the Production of H₂ Through the Water-Gas-Shift Reaction: Time-Resolved XRD and XAFS Studies. *Top. Catal.* **2008**, *49* (1–2), 81–88. https://doi.org/10.1007/s11244-008-9071-6.
- (81) Lykaki, M.; Pachatouridou, E.; Carabineiro, S. A. C.; Iliopoulou, E.; Andriopoulou, C.; Kallithrakas-Kontos, N.; Boghosian, S.; Konsolakis, M. Ceria Nanoparticles Shape Effects on the Structural Defects and Surface Chemistry: Implications in CO Oxidation by Cu/CeO₂ Catalysts. *Appl. Catal. B Environ.* **2018**, *230*, 18–28. https://doi.org/10.1016/j.apcatb.2018.02.035.
- (82) Wang, W.-W.; Du, P.-P.; Zou, S.-H.; He, H.-Y.; Wang, R.-X.; Jin, Z.; Shi, S.; Huang, Y.-Y.; Si, R.; Song, Q.-S.; et al. Highly Dispersed Copper Oxide Clusters as Active Species in Copper-Ceria Catalyst for Preferential Oxidation of Carbon Monoxide. *ACS Catal.* **2015**, *5* (4), 2088–2099. https://doi.org/10.1021/cs5014909.
- (83) Laguna, O. H.; Centeno, M. A.; Arzamendi, G.; Gandía, L. M.; Romero-Sarria, F.; Odriozola, J. A. Iron-Modified Ceria and Au/Ceria Catalysts for Total and Preferential Oxidation of CO (TOX and PROX). *Catal. Today* **2010**, *157* (1–4), 155–159. https://doi.org/10.1016/j.cattod.2010.04.011.
- (84) Aragao, I. B.; Bueno, J. M. C.; Zanchet, D. Platinum Clusters Deposited on Maghemite Applied to Preferential Oxidation of CO under Hydrogen Rich Conditions (PROX-CO). *Appl. Catal. A Gen.* **2018**, *568*, 86–94. https://doi.org/10.1016/j.apcata.2018.09.014.
- (85) Fiorenza, R.; Crisafulli, C.; Scirè, S. H₂ Purification through Preferential Oxidation of CO over Ceria Supported Bimetallic Au-Based Catalysts. *Int. J. Hydrogen Energy* **2016**, 1–9. https://doi.org/10.1016/j.ijhydene.2016.05.114.

ASSOCIATED CONTENT

Supporting Information.

The SI file presents the detailed experimental procedure and additional information about the characterization of the colloidal NPs and catalysts, and complementary catalytic results.

AUTHOR INFORMATION

Corresponding Author

*Institute of Chemistry, University of Campinas, P.O. Box 6154, Campinas-SP 13083-970,

Brazil. E-mail: zanchet@unicamp.br

Author Contributions

T.E.R. Fiuza and D. Zanchet conceived the idea of the project. T.E.R. Fiuza acquired the experimental data and performed the data analysis. D.Z. supervised the findings of this work. Both authors discussed the results and contributed to the final manuscript.

SYNOPSIS (GRAPHICAL ABSTRACT)

